# Solvent and Solvent Isotope Effects on the Vibrational Cooling Dynamics of a DNA Base Derivative

**Chris T. Middleton, Boiko Cohen,† and Bern Kohler***

*Department of Chemistry, The Ohio State University, 100 West 18th Avenue, Columbus, Ohio 43210*

*Received: May 25, 2007; In Final Form: July 21, 2007*

Vibrational cooling by 9-methyladenine was studied in a series of solvents by femtosecond transient absorption spectroscopy. Signals at UV and near-UV probe wavelengths were assigned to hot ground state population created by ultrafast internal conversion following electronic excitation by a 267 nm pump pulse. A characteristic time for vibrational cooling was determined from bleach recovery signals at 250 nm. This time increases progressively in $H_2O$ (2.4 ps), $D_2O$ (4.2 ps), methanol (4.5 ps), and acetonitrile (13.1 ps), revealing a pronounced solvent effect on the dissipation of excess vibrational energy. The trend also indicates that the rate of cooling is enhanced in solvents with a dense network of hydrogen bonds. The faster rate of cooling seen in $H_2O$ vs $D_2O$ is noteworthy in view of the similar hydrogen bonding and macroscopic thermal properties of both liquids. We propose that the solvent isotope effect arises from differences in the rates of solute−solvent vibrational energy transfer. Given the similarities of the vibrational friction spectra of $H_2O$ and $D_2O$ at low frequencies, the solvent isotope effect may indicate that a considerable portion of the excess energy decays by exciting relatively high frequency ($\geq$700 $cm^{-1}$) solvent modes.

## 1. Introduction

Vibrational cooling (VC) is the process by which a molecule with excess vibrational energy returns to thermal equilibrium with its surroundings. It plays an important role in photochemistry and photophysics because transitions between electronic states frequently leave a molecule with significant amounts of excess vibrational energy. There is longstanding interest in the intra- and intermolecular interactions that mediate vibrational energy redistribution and transfer because these processes drive the nuclear dynamics that underlie chemical reaction dynamics.[1,2] Despite intensive study, vibrational cooling is poorly understood. It is easy enough to describe vibrational cooling in phenomenological terms, but microscopic models have remained elusive. The solvent plays a complex role by facilitating intermolecular energy transfer and intramolecular energy redistribution, possibly on overlapping time scales. State-to-state energy-transfer rates can be measured in favorable cases for small molecules, but energy transfer by larger solutes takes place simultaneously via a large number of coupled vibrations. Further experiments are needed to delineate fundamental issues.

Knowledge about vibrational cooling has come primarily from time-resolved spectroscopy. Excess vibrational energy in a molecule in the condensed phase can be readily monitored through temperature-dependent changes in absorption line shapes.[1,3,4] To be detectable, the nonequilibrium energy distribution must be created faster than the time required for relaxation. Molecules that undergo ultrafast internal conversion to the electronic ground state ($S_0$) are thus ideal. Rapid nonradiative decay from an excited electronic state can easily create several electronvolts of excess vibrational energy. Additionally, vibrational relaxation is in principle easier to follow in $S_0$ where vibrational frequencies and anharmonicities are known more precisely than in excited electronic states. To date, a relatively small number of molecules that undergo ultrafast internal conversion have been used to investigate vibrational cooling. The most commonly studied molecules include azulene,[4−8] *p*-nitroaniline (PNA),[8−11] and polyenes such as *cis*-hexatriene[12] and $\beta$-carotene.[13] One purpose of this report is to introduce the DNA and RNA bases and their derivatives as useful model systems for studying vibrational cooling and the effects of hydrogen bonds on solute−solvent energy transfer. The short lifetimes (<1 ps [14]) of the $^1\pi\pi^*$ states of these compounds and their large transition energies abruptly deposit more than 4 eV of energy into vibrations in $S_0$. In previous studies, near-UV transient absorption signals from adenosine (Ado) and cytidine (Cyd) in $H_2O$[15] as well as from 1-cyclohexyluracil in various solvents[16] have been assigned to vibrational cooling. Vibrational cooling also occurs in oligonucleotides due to the presence of monomer-like relaxation[17,18] but is more difficult to observe because ultrafast internal conversion is just one of several nonradiative decay pathways. Monomeric nucleobases are readily soluble in aqueous solution, and their multiple hydrogen-bonding sites enable study of the influence of hydrogen bonds on vibrational energy flow in solution.

Here we report a femtosecond transient absorption study of solvent effects on vibrational cooling dynamics of the adenine derivative, 9-methyladenine (9MA). N9-substituted derivatives of adenine are outstanding model compounds for vibrational cooling studies because internal conversion occurs faster ($\tau \sim$ 300 fs) than for nearly any other nucleobase derivative and occurs with essentially 100% efficiency, as shown below. Our results indicate that cooling is strongly accelerated in aqueous solution compared to other solvents. Studies of hydrogen-bonded solutes such as betaine-30[19] and PNA[8−10] have shown that hydrogen bonds accelerate vibrational cooling, but the underlying reasons are unclear. Despite their similar macroscopic thermal properties vibrational cooling occurs 1.8 times more slowly in $D_2O$ than in $H_2O$. A solvent kinetic isotope effect

* Corresponding author: E-mail: kohler@chemistry.ohio-state.edu.
† Current address: Departamento de Quimica Fisica, Universidad de Castilla La Mancha, Avda. Carlos III, S.N., 45071 Toledo, Spain.

10.1021/jp0740595 CCC: $37.00 
Published on Web 10/02/2007

has been seen previously for vibrational cooling by PNA in water[9] and on vibrational population lifetimes in some triatomic ions.[20,21] In this paper, we have attempted to explain the observed solvent isotope effect in terms of the frequency-dependent vibrational friction of water. The effect suggests that a significant portion of the excess vibrational energy is relaxed in water via energy transfer between high-frequency (>700 $cm^{-1}$) solute and solvent modes.

## 2. Experimental Methods

Transient absorption experiments were performed with a femtosecond pump−probe spectrometer at The Ohio State University's Center for Chemical and Biophysical Dynamics. A Ti:sapphire oscillator and regenerative amplifier manufactured by Coherent Inc. (Santa Clara, CA) produced femtosecond pulses with a center wavelength of 800 nm at a repetition rate of 1 kHz. This output was split to create pump and probe pulses. The pump pulse at 267 nm was generated by mixing the fundamental and second harmonic of the amplified pulses. Tunable probe pulses between 250 and 285 nm were generated via the second harmonic of the sum frequency of the signal beam from an optical parametric amplifier and a fundamental beam. After passing through the sample, the probe beam was spectrally filtered using a double monochromator and detected with a PMT. Visible probe signals at 570 and 600 nm were obtained by overlapping a white light continuum generated in a 1 cm water cell with the pump pulse in the sample, and spectrally filtering the continuum pulse after the sample using a 10 nm bandpass interference filter. Signals were measured by a lock-in amplifier, referenced to the frequency of an optical chopper placed in the pump beam.

Sample solutions were held in a home-built spinning cell with $CaF_2$ windows and a path length of 1.2 mm. The cell was rotated about an axis perpendicular to the windows fast enough that successive pump pulses did not excite the same sample volume. Sample concentrations were adjusted to have an absorbance of 1.0 at the pump wavelength. 9-Methyladenine was used as received from Sigma-Aldrich (St. Louis, MO). $H_2O$ was obtained from a water ultrapurification system (Barnstead International, Dubuque, IA). Buffer solutions were made at pH 7 using an equal molal mixture of $Na_2HPO_4$ and $KH_2PO_4$ in $H_2O$ ($3.4 \times 10^{-3}$ *m* each). $D_2O$ (Sigma-Aldrich, 99.9% D atom purity) was used unbuffered. Transient signals measured in buffered and unbuffered $H_2O$ solutions were identical within experimental uncertainty, indicating that the absence of buffer in $D_2O$ is of no consequence. Measurements on $D_2O$ samples were performed immediately after preparation to minimize exchange with $H_2O$ present in air. Acetonitrile and methanol were used as obtained from Sigma-Aldrich.

Multiphoton ionization of $H_2O$ and methanol by the pump pulse causes long-lived signals due to absorption by solvated electrons. These were removed from visible wavelength transients by subtracting the signal measured for the solvent by itself, scaled to match at long delay times, as previously described.[22] For probe wavelengths below 300 nm no correction for solvent ionization was necessary, but a prominent positive spike was caused by two-photon absorption (TPA) when pump and probe pulses overlap temporally in the sample. Following Reuther et al.,[23] this feature was used to estimate the precise location of zero delay time and the instrument response function (IRF, ∼250 fs). Signal was acquired for each sample by averaging between 5 and 10 scans. The standard deviation at each delay time was calculated from the data and used as a weighting factor in the fitting routine. Back-to-back measurements were made of the sample and neat solvent. The weighted average for both the sample and solvent were globally fit to their respective model functions. For the sample, this was a sum of exponentials plus a $\delta$ function at zero delay time. For the solvent, a $\delta$ function at time zero was used. For both, the model function was convoluted with a Gaussian function that represents the IRF. Since they were acquired under the same experimental conditions, zero delay time and the width of the IRF were linked between the two data sets. For each sample, solvent-subtracted decays at 570 and 600 nm were globally fit to a single time constant. In all figures below, the data are presented along with best-fit curves (solid lines) calculated from the fitting parameters. For clarity, the component of the fit corresponding to the time zero spike has been removed from the best-fit curves. All reported errors are twice the standard error.

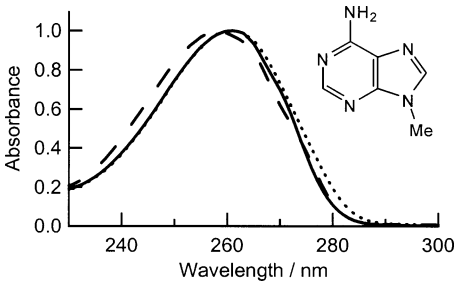


**Figure 1.** Normalized ground state absorption spectra of 9MA in $H_2O$ (solid line), methanol (dotted line), and acetonitrile (dashed line). The chemical structure of 9MA is also shown.

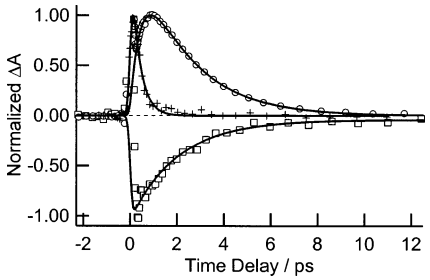


**Figure 2.** Transient absorption recorded for 9MA in $H_2O$, probed at 570 (crosses), 285 (circles), and 255 nm (squares), following excitation at 267 nm. Solid lines are fits to data as described in text.

## 3. Results

**3.1. Solvent-Dependent Absorption Spectra.** Ground-state absorption spectra of 9MA in $H_2O$, methanol, and acetonitrile are shown in Figure 1. The band maximum occurs at 261 nm in $H_2O$ and methanol and at 258 nm in acetonitrile. The band full width at half-maximum is 29 nm in $H_2O$, 30 nm in methanol, and 31 nm in acetonitrile. Identical band shapes are observed in $H_2O$ and $D_2O$, but the spectrum in heavy water is shifted by ∼0.5 nm to shorter wavelength. These spectra show that solvent effects on the room-temperature absorption spectra are very modest.

**3.2. Vibrational Dynamics in $H_2O$.** Normalized transient absorption signals for 9MA in $H_2O$ at several probe wavelengths are shown in Figure 2. At 570 nm, an instrument-limited rise is followed by a decay with a time constant of 0.36 ps, in good agreement with the lifetime reported by Cohen et al.[22] Best-fit parameter values for all 9MA transients are summarized in Table 1. Signals at 570 nm and other visible wavelengths are assigned to excited-state absorption by a $^1\pi\pi^*$ state.[14,15,22,24] The decay of this absorption is due to ultrafast internal conversion to $S_0$.[14]

The signal at 255 nm for 9MA in $H_2O$ is negative due to bleaching of the $S_0$ population by the pump pulse. The bleaching

**TABLE 1: Time Constants from Least-Squares Fits to 9MA Measurements[a]**

| solvent | probe wavelength (nm) | $\tau_1$ (ps) | $\tau_2$ (ps) |
|---|---|---|---|
| acetonitrile | 250 | $2.10 \pm 0.07$ | $13.1 \pm 0.06$ |
| methanol | 250 | $1.0 \pm 0.6$ | $4.5 \pm 0.6$ |
| $D_2O$ | 250 | $0.3 \pm 0.5$ | $4.2 \pm 1.6$ |
| $H_2O$ | 250 | $0.5 \pm 0.2$ | $2.4 \pm 0.4$ |
| $D_2O$ | 255 | | $3.4 \pm 0.3$ |
| $H_2O$ | 255 | | $2.0 \pm 0.2$ |
| $D_2O$ | 285 | $0.35 \pm 0.09$ | $3.9 \pm 0.5$ |
| $H_2O$ | 285 | $0.47 \pm 0.06$ | $2.11 \pm 0.12$ |
| $H_2O$ | 570, 600 | $0.36 \pm 0.03$ | |
| $D_2O$ | 570, 600 | $0.34 \pm 0.04$ | |
| methanol | 570, 600 | $0.43 \pm 0.05$ | |
| acetonitrile | 570, 600 | $0.410 \pm 0.014$ | |

[a] Uncertainties are equal to twice the standard error.

signal subsequently recovers with a time constant of $2.0 \pm 0.2$ ps, returning completely to the baseline 10 ps after the pump pulse. This signal recovers to the baseline about six times more slowly than signals at visible probe wavelengths, indicating that different states are probed. The absence of slow relaxation channels indicates that all photoexcited 9MA molecules decay to $S_0$ via ultrafast IC. In contrast, only 50−90% of photoexcited pyrimidine bases decay via ultrafast internal conversion in aqueous solution due to branching to a $^1n\pi^*$ state.[16,25] The signal at 285 nm shows more complex dynamics. There is little $S_0$ absorption at room temperature at this wavelength (Figure 1), and no bleaching is observed at any delay time. The signal rises with a time constant of 0.47 ps. This value is somewhat longer than the time constant measured at 570 nm. After reaching a maximum near 1 ps, the 285 nm signal decays to the baseline with a time constant of $2.11 \pm 0.12$ ps in good agreement with the decay time observed at 255 nm.

The UV signals monitor the effect of temperature on absorption by molecules in the $S_0$ state.[14,15] More precisely, the UV signals reflect changes to the ground-state absorption spectrum caused by excess vibrational energy in the Franck−Condon active vibrational modes. Vibrational cooling generally requires no more than a few tens of picoseconds in solution[1] and is therefore observable only when internal conversion takes place more rapidly.

Scaled transient absorption signals at 250 and 255 nm are compared in Figure 3. After 2 or 3 ps, both signals decay at the same rate within experimental uncertainty. At shorter delay times, a faster decay component with positive amplitude is seen at 250 nm, which is not present at 255 nm. The same behavior was seen in methanol and acetonitrile. In each solvent, the faster of the two decay components seen at 250 nm ($\tau_1$ in Table 1) is greater than the time constant for internal conversion measured at 570 and 600 nm.

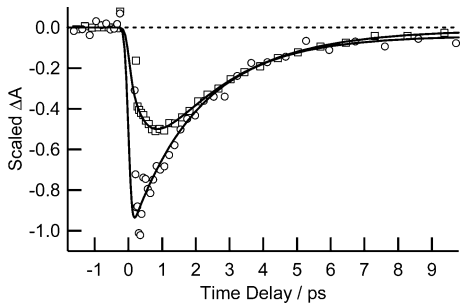


**Figure 3.** Transient absorption of 9MA in $H_2O$ at probe wavelengths of 255 (circles) and 250 nm (squares), following excitation at 267 nm. Signals have been scaled for agreement at delay times greater than 3 ps. Solid lines are fits to data as described in text.

**TABLE 2: Comparison of Vibrational Cooling (VC) Rates for 9MA in $H_2O$, $D_2O$, Methanol, and Acetonitrile with Select Solvent Macroscopic Properties**

| | $H_2O$ | $D_2O$ | methanol | acetonitrile |
|---|---|---|---|---|
| relative rate of VC[a] | 5.5 | 3.1 | 2.9 | 1 |
| thermal diffusivity[b] ($10^{-8}$ m$^2$ s$^{-1}$) | 14.3 | 12.7 | 10.1 | 10.7 |
| thermal conductivity[c] (W m$^{-1}$ K$^{-1}$) | 0.61 | 0.59 | 0.20 | 0.19 |
| density[c] (g mL$^{-1}$) | 1.00 | 1.10 | 0.79 | 0.78 |
| OH (OD) bond density[d] (mol mL$^{-1}$) | 0.11 | 0.11 | 0.03 | 0 |

[a] Calculated using $\tau_2$ from Table 1 at 250 nm. [b] Data for $D_2O$ from ref 61; others from ref 60. [c] Data for $D_2O$ from ref 62; others from ref 63. [d] Calculated as in ref 19.

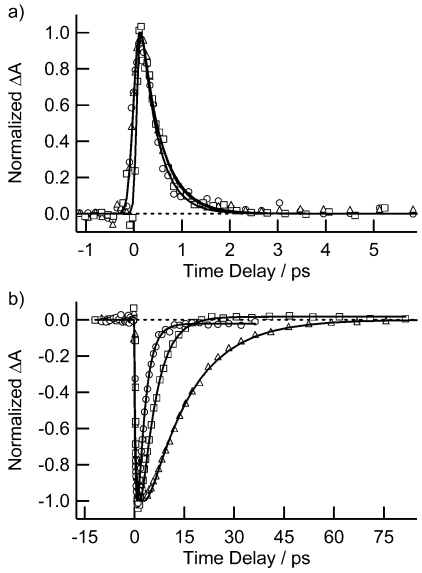


**Figure 4.** Transient absorption of 9MA in $H_2O$ (circles), methanol (squares), and acetonitrile (triangles) following excitation at 267 nm. (a) Probe wavelength of 570 nm, corrected for signal from solvated electron as described in text. (b) Probe wavelength of 250 nm. Solid lines are fits to data as described in text.

**3.3. Dynamics in Other Solvents.** Transients were recorded in $D_2O$, methanol, and acetonitrile to investigate solvent effects on vibrational cooling. The signals at 570 nm depend weakly on solvent (see Figure 4a and Table 1), and the decay times in acetonitrile (0.41 ps) and methanol (0.43 ps) are only slightly longer than in $H_2O$ (0.36 ps). The signal in $D_2O$ at 570 nm is indistinguishable from the one in $H_2O$ at the same probe wavelength (Table 1). These observations indicate that internal conversion occurs at an essentially solvent-independent rate. Identical rates of internal conversion in $H_2O$ and $D_2O$ were previously reported for adenine.[22] The identical decays seen in $H_2O$ and $D_2O$ make it unlikely that nonradiative decay takes place via excited-state proton or hydrogen atom transfer.[22] Although there is a negligible solvent effect on internal conversion, the bleach recovery signals at 250 nm are highly sensitive to solvent with a 5-fold increase in the lifetime at 250 nm on going from $H_2O$ to acetonitrile (Figure 4b). This sensitivity to solvent is a well-known signature of vibrational cooling dynamics[19,26,27] and confirms the earlier assignment[15,24] of the near-UV signals to hot ground state molecules formed by ultrafast internal conversion.

Transient signals at 255 and 285 nm are shown in Figure 5 for 9MA in $H_2O$ and $D_2O$. The solute in the latter solvent is 9MA-$d_2$ due to exchange of the two hydrogen atoms of the amino group. Time constants for 9MA-$d_2$ in $D_2O$ are about 1.8 times longer than ones for 9MA in $H_2O$ (Table 1). This

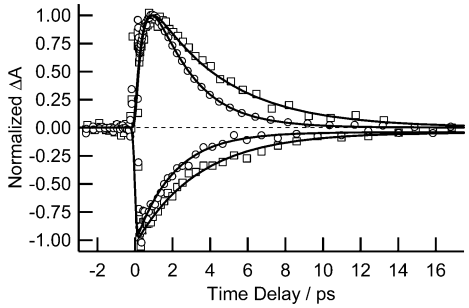


**Figure 5.** Transient absorption of 9MA in $H_2O$ (circles) and $D_2O$ (squares) at 255 (negative $\Delta A$) and 285 nm (positive $\Delta A$). Solid lines are fits to data as described in text.

significant isotope effect is the main finding of this work. Because there is no isotope effect on the rate of internal conversion (vide supra), the results in Figure 5 are assignable to vibrational cooling dynamics. The aim of the next section is to discuss what the observed isotope effect reveals about vibrational relaxation.

## 4. Discussion

**4.1. Hot Band Evolution and Phenomenological Cooling Rates.** Excess vibrational energy dramatically alters the ground-state absorption band of 9MA, leading to spectral broadening, decreased absorption near the room-temperature band maximum, and increased absorption at longer wavelengths, as seen in other chromophores.[4,6,9,28−31] As the hot solute molecule returns to thermal equilibrium with the cooler surrounding solvent molecules, the $S_0$ spectrum changes in response to intra- and intermolecular energy transfer. Empirically, transient absorption signals from molecules undergoing vibrational cooling have been observed to decay in monoexponential[4,29,32] or biexponential[9,33] fashion at discrete probe wavelengths. Because dynamic band shifting and band narrowing take place, the observed lifetimes depend on the spectral position of the probe pulse within the absorption band. Usually, faster decays are observed at longer probe wavelengths.[4,26,29,32]

It is difficult to extract rate constants for elementary relaxation processes from the many time constants that characterize the complex evolution of the ground-state absorption band. Some have attempted to do this by modeling the temperature dependence of the absorption spectrum.[9,31,34] In favorable cases, this has yielded estimates of the rate of decay of the microcanonical temperature[9,30] or excess vibrational energy.[31,34] Given the nonlinear dependence of the molecular absorption coefficient on temperature, and the many assumptions that underlie these analyses, we have followed a simpler procedure. We have chosen the value of $\tau_2$ at 250 nm as a phenomenological estimate of the vibrational cooling time and have used this to calculate the relative rates in Table 2.

Vibrational cooling has usually been monitored by measuring transient absorption signals within the long-wavelength tail of the absorption band of interest.[4,30−32] Bleach recovery signals like the ones we have recorded at 250 nm also report on vibrational cooling due to the reduction of the absorption cross section near the band maximum at elevated temperatures. Kovalenko et al. made a similar observation in their broadband transient absorption study of PNA.[9] The time constant of ~2 ps ($\tau_2$ in Table 1) observed for the bleach recovery signals at 250 nm in $H_2O$ agrees within experimental uncertainty with the value of $\tau_2$ at 285 nm. The measured time constants are relatively independent of probe wavelength near 250 and 290 nm, but shorter time constants are observed at longer wavelengths. Decay times for adenosine in $H_2O$ were previously found to decrease from 2.0 ps at 270 nm to 0.4 ps at 340 nm.[15]

Recently, Kwok et al. reported a second excited-state absorption band of the $^1\pi\pi^*$ state of adenosine with a maximum near 350 nm in aqueous solution.[35] Like the excited-state absorption band first seen at visible wavelengths,[15] this band decays on a sub-picosecond time scale. Thus, although the faster decays at longer wavelengths are partially attributable to accelerated cooling at smaller transition frequencies,[4,26] the sub-picosecond decay of the $^1\pi\pi^*$ state also contributes to the dynamics. The difficulty of disentangling vibrational cooling and internal conversion dynamics at wavelengths longer than 300 nm in adenine derivatives is another reason for using the bleach recovery signals at 250 nm as a measure of vibrational cooling rates. Compared to other probe wavelengths, the signals near the band maximum are the last ones to fully return to the baseline, making the decay time at 250 nm a good measure of the maximum amount of time needed for complete recovery of the ground-state spectrum. The absorption spectrum of 9MA is virtually the same in all solvents, so the energy difference between the origin of the electronic transition in a given solvent and the probe wavelength is approximately constant. As a result, the 250 nm signal recovery time is a robust estimate of how cooling varies with solvent—our main interest in this study.

There is a significant difference between the transients at 250 and 255 nm at short delay times (Figure 3). At 250 nm, two exponentials with amplitudes of opposite sign are needed to fit the transient signals, while the 255 nm signal decays monoexponentially. In principle, bleach recovery signals contain a decay component due to internal conversion. This component has a positive amplitude like that of the faster decay component seen in Figure 3 ($\tau_1$ in Table 1). However, this lifetime is longer than the internal conversion time in each solvent. Furthermore, it depends sensitively on solvent unlike the rate of internal conversion. Any signal contribution from internal conversion is also expected to be weak and difficult to observe because the rate of internal conversion is considerably faster than the rate of cooling.

We propose instead that the signal at 250 nm, but not at 255 nm, detects hot band absorption on the far-red wing of the strong $S_0$ absorption band centered near 200 nm. The rise of the hot band is likely not observed because of our limited time resolution and overlapping contributions from the time-zero spike and ground-state bleaching. Therefore, the 250 nm signal contains contributions from the thermalization of two ground-state bands. The underlying thermalization dynamics are only apparently different due to the unequal energy offsets between the probe wavelength and the electronic origin of each transition. Different absorption bands of the same chromophore have also been reported to undergo vibrational cooling at different rates,[36] and this possibility cannot be ruled out. The 255 nm signals presumably do not show the hot ground state absorption by the higher energy absorption band because its amplitude and time constant are both expected to decrease at longer probe wavelengths. Transient dichroism measurements could answer the question of whether two distinct electronic transitions are observed in this spectral region.

Transient absorption experiments such as ours are sensitive to average populations in Franck−Condon active modes in $S_0$. These populations can change via intermolecular energy transfer, which must ultimately take place for the hot solute molecule to return to equilibrium with the solvent, or by intramolecular vibrational redistribution (IVR). We consider next whether the observed decays can be assigned to IVR. Here, we understand IVR to mean processes that promote the attainment of Boltz-

mann populations with minimal energy transfer to the solvent. Solvent-assisted IVR can transfer significant amounts of energy to the solvent and will be considered later.

The signal at 285 nm puts some constraints on possible IVR processes. This signal is assigned to hot ground state absorption since there is negligible absorption by 9MA at room temperature at this wavelength (Figure 1). The rise time therefore measures the time required for excess vibrational energy to appear in the Franck−Condon active modes of $S_0$. Bingemann et al.[30] and later Charvat et al.[31] observed rise-and-fall kinetics in transient absorption signals recorded on the red edge of the ground-state absorption spectrum of vibrationally excited methylene iodide in nonpolar solvents.[30] In those experiments, vibrational excitation was provided by overtone excitation of C−H stretching vibrations. Because such modes are Franck−Condon inactive, the observed rise time of ∼10 ps was assigned to the time needed to re-distribute energy from the C−H stretch to Franck−Condon active modes.

In our experiments, the rise time at 285 nm agrees within experimental uncertainty with the decay time of the excited-state absorption at 570 nm in both $H_2O$ and $D_2O$. Hot ground state absorption is not expected to appear any earlier due to the delay introduced by internal conversion of the photoexcited molecules. The agreement of the rise time with the internal conversion time suggests either that IVR is complete in less than 300 fs or that at least some of the modes excited during internal conversion (the accepting modes for nonradiative decay) are also Franck−Condon active in $S_0$. In this case, the hot band absorption signals would rise with the excited-state lifetime even if IVR takes place slowly. Calculations by Matsika on uracil show that ring stretching modes and out-of-plane modes are active near the conical intersection responsible for nonradiative decay.[37] The former modes have substantial Franck−Condon activity, suggesting that they could be directly excited by internal conversion, as opposed to indirectly via IVR. Thus, either a number of the Franck−Condon active modes in $S_0$ directly accept vibrational energy during internal conversion or they are populated by IVR from the actual accepting modes in less time than is required for internal conversion.

The contribution of IVR to vibrational cooling signals is uncertain. Internal conversion from an excited electronic state creates an unknown distribution of excited vibrations, making it impossible to measure state-specific relaxation rates. Many workers have assumed that IVR produces Boltzmann-distributed vibrational populations before any significant energy transfer to the solvent takes place.[1,4,30,31] However, recent work has shown that the IVR mechanism operative in the gas phase, i.e., relaxation via tiers of coupled states, is observable in solution.[38,39] Abel and co-workers have argued from their experiments on aromatic molecules like benzene and pyrazine in weakly interacting solvents that IVR between certain tiers of states can lead to IVR on the time scale of a few picoseconds.[40,41] It remains to be shown that slow IVR is possible at the much higher vibrational energies of our experiments, but the speed of vibrational cooling by 9MA in water suggests that vibrational energy transfer to the solvent could take place concurrently with IVR. In the remaining discussion, we will neglect this possibility and assume that the observed signal decays are determined primarily by intermolecular energy transfer.

**4.2. Solvent Effects on Vibrational Cooling.** Comparison of the lifetimes measured in protic and aprotic polar solvents (Table 1) indicates that vibrational cooling is strongly accelerated in hydrogen bonding solvents, as seen in previous studies.[6,9,19] It is unknown in detail how hydrogen bonds promote vibrational cooling. During vibrational cooling energy is transferred from the hot solute to cooler molecules in the first solvent shell and eventually to more distant solvent molecules. Sukowski et al.[26] proposed that energy transfer in the first step is due to isolated binary collisions and used macroscopic heat conduction to model the second step. In weakly coupled solvents, solvent−solvent energy transfer has been suggested to be the rate-limiting step from the observed dependence of the cooling rate on the thermal diffusivity of the solvent.[9,27,36,42] Despite this success, the sole use of the thermal diffusivity to model vibrational cooling rates has been criticized because it fails to reproduce the experimental dependence on solvent density.[6] As shown in Table 2, the thermal diffusivities for the solvents in our study are poorly correlated with the observed vibrational cooling rates, particularly in water. From this result and from the ability of vibrational energy to spread through water on a sub-picosecond time scale,[43,44] we conclude that solvent−solvent energy transfer is not the main reason for accelerated vibrational cooling in hydrogen-bonding solvents.

We suggest that rapid vibrational cooling is due to the ability of hydrogen bonds to promote rapid energy transfer from the hot solute to molecules in the first solvent shell. The high density of collective motions (translations and intermolecular vibrations) in water facilitates this energy transfer, but the anharmonicity of hydrogen bonds is also important.[45] An excellent example of the latter effect is a study by Ernsting and co-workers of vibrational cooling of PNA.[9] In this study, the band integral of the hot ground state spectrum of PNA was observed to decay more rapidly than that of (dimethylamino)-*p*-nitroaniline in a series of alcohol solvents, but similar decay rates were observed in acetonitrile. Dimethylation of the amino group of PNA reduces the number of solute−solvent hydrogen bonds, leading to slower vibrational cooling in the protic solvents.

Terazima provided a qualitative metric for assessing the effect of hydrogen bonds on vibrational cooling. He observed comparable cooling rates for betaine-30 in aprotic solvents, but 3−5 times faster rates in protic solvents.[19] Furthermore, the rate of cooling in a series of alcohol solvents did not scale with the thermal diffusivity but was reasonably well correlated with the number density of solvent OH groups.[19] Our results show that vibrational cooling rates differ in $H_2O$ and $D_2O$ by nearly a factor of 2, even though these solvents have the same OH/OD bond density (Table 2).

**4.3. Solvent Isotope Effect.** A solvent isotope effect on vibrational dynamics has been seen previously for a small number of molecules. It was found for vibrational cooling of PNA[9] and vibrational population relaxation of specific modes of some triatomic species.[20,21] Previously, we observed that transient absorption at 340 nm by 1-cyclohexyluracil decays 1.3 times more slowly in $D_2O$ than in $H_2O$.[16] PNA is the most similar of these molecules to 9MA. Both compounds undergo ultrafast internal conversion in ∼0.3 ps in $H_2O$ and $D_2O$. Both have multiple hydrogen-bonding sites (≥4) and a similar number of internal degrees of freedom: PNA has 42 normal modes, while 9MA has 48. In $D_2O$, the amino group of each compound is fully deuterated. It is informative then to compare the relaxation times measured by Kovalenko et al.[9] for PNA with our results for 9MA. Kovalenko et al. fit the decay of the integrated band shape to a biexponential function.[9] On the other hand, our signals are adequately described by a single-exponential decay. To facilitate comparison, we have computed amplitude-averaged time constants, $\langle\tau\rangle = \sum_{i=1}^{2} A_i\tau_i$, from the normalized amplitudes, $A_i$, and time constants, $\tau_i$, given in Table

1 of ref 9. The results are 1.5 ps for $H_2O$ and 2.6 ps in $D_2O$. The faster decay seen for PNA vs 9MA may be due to the 50% increase in excess vibrational energy in our experiments. The solvent isotope effect of 1.8 for PNA is nearly the same as the one reported here for 9MA, suggesting that they share a common origin.

Kovalenko et al. proposed that energy transfer from a hot solute molecule to molecules in the first solvent shell occurs via rapid energy transfer to strongly coupled "active molecules" in addition to slower transfer to more weakly coupled molecules.[9] Strongly coupled molecules were suggested by the authors to be ones that are hydrogen bonded to the solute. Using a model with many adjustable parameters, they were able to reproduce the slower rate of cooling in $D_2O$, but only by assuming that there are 30% fewer strongly coupled (i.e., hydrogen-bonded) molecules in the first solvent shell in $D_2O$ than in $H_2O$. This unrealistic change in the number of nearest-neighbor molecules and the complexity of their model led us to seek an alternative, microscopic explanation.

It is important to remember that the solute in our experiments in $D_2O$ is actually 9MA-$d_2$ due to exchange of the amino group hydrogens. The isotope effect might therefore be explained trivially by a change in solute frequencies. Overall, normal-mode frequencies calculated for 9MA and 9MA-$d_2$ in the gas phase are very similar, and only 6 of 48 normal modes change in frequency by more than 10%.[46] The similar frequencies result in just a 1% difference in the initial vibrational temperature calculated from the vibrational partition function (see Supporting Information). Furthermore, resonance Raman data for adenine 5′-mononucleotide in $H_2O$ and $D_2O$ show only slight changes in the frequencies of the Franck−Condon active modes.[47] This evidence strongly indicates that ground-state absorption by 9MA and 9MA-$d_2$ should depend nearly identically on temperature. Changes in solute frequencies upon deuteration could also affect IVR pathways, which could lead to an isotope effect if IVR were the rate-limiting step. However, the vibrational cooling rate is proposed to be limited by the rate of energy transfer to the solvent, as discussed earlier. We conclude that the isotope effect is due overwhelmingly to changes in solvent frequencies.

**4.4. Microscopic Descriptions of Intermolecular Vibrational Energy Transfer.** Vibrational cooling is frequently discussed as taking place via a "vibrational cascade" in which intramolecular vibrations decay to lower frequency ones, releasing the energy difference into a small number of low-frequency bath phonons.[48,49] Bath modes accept just enough energy to redistribute vibrational energy from higher frequency to lower frequency intramolecular modes. The high density of low-frequency bath states is thought to make descent of the ladder of intramolecular vibrational states in many small steps highly efficient. A second relaxation process involves the direct transfer of energy from an intramolecular vibration to a solvent mode of the same frequency. There is considerable uncertainty about which process is more important.[50] Both have been suggested to contribute to vibrational relaxation of the azide ion[51] and pseudo-halide anions.[21] Computer simulations further indicate that both mechanisms exhibit an isotope effect in water when the solvent mode has a sufficiently high frequency.[51]

Vibrational energy transfer to bath modes can be understood in terms of the fluctuating forces solvent molecules exert on the solute. Vibrational friction arising from these forces dampens vibrational motion and induces energy transfer.[2,50] According to perturbation theory, the rate of transfer is equal to the product of a coupling term and the magnitude of the force−force autocorrelation function at the frequency of the relaxing mode.[2] We shall assume that this perturbation-theory perspective is still applicable to strongly coupled solute−solvent systems like 9MA in water. The forces pertinent to a solute mode of a given frequency and vibrational coordinate are those that fluctuate at the same frequency and along the same coordinate. The friction is greatest at low frequency and decreases approximately exponentially with increasing frequency. Additionally, the friction is enhanced at the frequencies of intramolecular solvent vibrations. These vibrations dominate the friction spectrum at high frequency where collective solvent modes are absent.

We consider next whether the observed isotope effect can be explained by differences in the friction spectra of $H_2O$ and $D_2O$. Friction spectra for these solvents have been evaluated from molecular dynamics simulations of hydrated $CN^-$,[52] $ClO^-$,[53] and OClO.[54] Although the friction spectrum of the solvent depends in principle on the nature of the solute, the spectra evaluated in water are relatively independent of the molecular identity of the solute. At frequencies below ~700 $cm^{-1}$ the vibrational friction spectra of $H_2O$ and $D_2O$ are nearly identical for a number of solutes.[52−54] This is reasonable since many of the low-frequency modes in this spectral region arise from hindered translations,[48] which differ insignificantly in frequency due to the similar molecular masses and intermolecular forces of $H_2O$ and $D_2O$. On the other hand, the friction spectra of $H_2O$ and $D_2O$ differ significantly at frequencies above ~700 $cm^{-1}$.[52−54] Here, the differences are due to the isotope effect on the frequencies of librations and intramolecular solvent vibrations. The ratio of librational frequencies in $H_2O$ and $D_2O$ is proportional to the square root of the moments of inertia, $(I_{H_2O}/I_{D_2O})^{1/2}$, a quantity which varies between 0.71 and 0.75, depending on the rotational axis. Intramolecular solvent vibrations in $D_2O$ are reduced in frequency by a similar factor because of reduced mass changes.

On the basis of these trends, we propose that the kinetic isotope effect for vibrational cooling of 9MA in water arises from energy transfer between solute and solvent modes with relatively high frequencies, i.e., energies ≥700 $cm^{-1}$. Librational modes between 700 and approximately 1000 $cm^{-1}$ are likely to be most important. In this frequency range, the friction is still sizable compared to the friction at lower frequencies. The presence of relatively high-frequency librational modes could explain the accelerated vibrational cooling seen in hydrogen bonding solvents. Such modes can rapidly down-convert energy from the many 9MA modes that lie between 1400 and 1800 $cm^{-1}$. As described above, Franck−Condon active modes like the ones in this region may carry most of the excess vibrational energy at times before IVR has completed.

Measurements of direct vibrational energy transfer from diatomic solutes to the solvent show that high-frequency vibrations relax more slowly in $D_2O$ than in $H_2O$. Thus, $CN^-$ with a frequency near 2000 $cm^{-1}$ exhibits a pronounced solvent isotope effect in water,[55] but $ClO^-$, which has a fundamental frequency of 713 $cm^{-1}$, does not.[53] Identical vibrational relaxation rates were observed for $I_2^-$ (113 $cm^{-1}$) in ethanol and ethanol-$d_1$.[56] and vibrational relaxation by $I_2$ in the electronic ground state has been shown to be independent of solvent deuteration.[57] These trends in molecules that cannot undergo IVR support our assignment of the isotope effect to energy transfer between higher frequency modes of 9MA and water.

## 5. Conclusions

Transient absorption by 9MA in the UV following excitation at 267 nm has been measured and assigned to vibrational cooling

of the hot ground state formed following ultrafast internal conversion. A strong solvent effect on the vibrational cooling rate was observed that is poorly correlated with macroscopic properties of the solvent. Instead, hydrogen-bonding properties of the solvent play a major role in the relaxation of excess vibrational energy. This chromophore dissipates approximately 37 000 $cm^{-1}$ of excess vibrational energy to surrounding $H_2O$ molecules with remarkable speed as judged by the full recovery of the ground-state absorption spectrum with a time constant of ca. 2 ps. This recovery, which we have assigned to vibrational energy transfer to the solvent, occurs 80% more slowly in $D_2O$ than in $H_2O$ solution. This result and a similar finding by Kovalenko et al. in their study of PNA[9] suggest that a solvent isotope effect is a general feature of vibrational cooling in aromatic molecules. Although a microscopic explanation cannot be established with certainty at this time, we have proposed that the nearly identical vibrational friction spectra of $H_2O$ and $D_2O$ at frequencies less than about 700 $cm^{-1}$ rule out cooling by intermolecular energy transfer from solute to solvent via just the lowest frequency solute modes.

Identical rates of internal conversion were measured for 9MA in $H_2O$ and $D_2O$, suggesting that the presence of an isotope effect may be a useful mechanism for distinguishing vibrational cooling from electronic relaxation. This could be particularly useful in studies of oligonucleotides where different excited-state decay pathways have been proposed.[17,58] Of course, a base in the DNA double helix experiences a very different environment than a single base in aqueous solution. In the former case, restricted access by solvent molecules and base pairing and stacking interactions with neighbors can strongly influence vibrational relaxation.[59] In this light, the present study of vibrational energy flow of single, solvated bases is a preliminary step toward understanding vibrational dynamics in these more complex systems.

**Acknowledgment.** This research was made possible by a grant from the National Institutes of Health (R01 GM64563). Measurements were performed in Ohio State's Center for Chemical and Biophysical Dynamics, using equipment funded by the National Science Foundation (CHE-0234684) and the Ohio Board of Regents.

**Supporting Information Available:** Description of the method used to assign the initial vibrational temperature following internal conversion. This material is available free of charge via the Internet at http://pubs.acs.org

## References and Notes

(1) Elsaesser, T.; Kaiser, W. *Annu. Rev. Phys. Chem.* **1991**, *42*, 83.
(2) Owrutsky, J. C.; Raftery, D.; Hochstrasser, R. M. *Annu. Rev. Phys. Chem.* **1994**, *45*, 519.
(3) Doany, F. E.; Greene, B. I.; Hochstrasser, R. M. *Chem. Phys. Lett.* **1980**, *75*, 206.
(4) Wild, W.; Seilmeier, A.; Gottfried, N. H.; Kaiser, W. *Chem. Phys. Lett.* **1985**, *119*, 259.
(5) Schwarzer, D.; Troe, J.; Schroeder, J. *Ber. Bunsen-Ges. Phys. Chem.* **1991**, *95*, 933.
(6) Schwarzer, D.; Troe, J.; Votsmeier, M.; Zerezke, M. *J. Chem. Phys.* **1996**, *105*, 3121.
(7) Okazaki, T.; Hirota, N.; Nagata, T.; Osuka, A.; Terazima, M. *J. Phys. Chem. A* **1999**, *103*, 9591.
(8) Kimura, Y.; Fukuda, M.; Kajimoto, O.; Terazima, M. *J. Chem. Phys.* **2006**, *125*, 194615.
(9) Kovalenko, S. A.; Schanz, R.; Hennig, H.; Ernsting, N. P. *J. Chem. Phys.* **2001**, *115*, 3256.
(10) Kozich, V.; Werncke, W.; Vodchits, A. I.; Dreyer, J. *J. Chem. Phys.* **2003**, *118*, 1808.
(11) Schrader, T.; Sieg, A.; Koller, F.; Schreier, W.; An, Q.; Zinth, W.; Gilch, P. *Chem. Phys. Lett.* **2004**, *392*, 358.
(12) Pullen, S. H.; Anderson, N. A.; Walker, L. A., II; Sension, R. J. *J. Chem. Phys.* **1997**, *107*, 4985.
(13) Siebert, T.; Maksimenka, R.; Materny, A.; Engel, V.; Kiefer, W.; Schmitt, M. *J. Raman Spectrosc.* **2002**, *33*, 844.
(14) Crespo-Hernández, C. E.; Cohen, B.; Hare, P. M.; Kohler, B. *Chem. Rev.* **2004**, *104*, 1977.
(15) Pecourt, J.-M. L.; Peon, J.; Kohler, B. *J. Am. Chem. Soc.* **2001**, *123*, 10370.
(16) Hare, P. M.; Crespo-Hernández, C. E.; Kohler, B. *J. Phys. Chem. B* **2006**, *110*, 18641.
(17) Crespo-Hernández, C. E.; Cohen, B.; Kohler, B. *Nature* **2005**, *436*, 1141.
(18) Schreier, W. J.; Schrader, T. E.; Koller, F. O.; Gilch, P.; Crespo-Hernández, C. E.; Swaminathan, V. N.; Carell, T.; Zinth, W.; Kohler, B. *Science* **2007**, *315*, 625.
(19) Terazima, M. *Chem. Phys. Lett.* **1999**, *305*, 189.
(20) Li, M.; Owrutsky, J.; Sarisky, M.; Culver, J. P.; Yodh, A.; Hochstrasser, R. M. *J. Chem. Phys.* **1993**, *98*, 5499.
(21) Lenchenkov, V.; She, C. X.; Lian, T. *J. Phys. Chem. B* **2006**, *110*, 19990.
(22) Cohen, B.; Hare, P. M.; Kohler, B. *J. Am. Chem. Soc.* **2003**, *125*, 13594.
(23) Reuther, A.; Laubereau, A.; Nikogosyan, D. N. *Opt. Commun.* **1997**, *141*, 180.
(24) Pecourt, J.-M. L.; Peon, J.; Kohler, B. *J. Am. Chem. Soc.* **2000**, *122*, 9348.
(25) Hare, P. M.; Crespo-Hernández, C. E.; Kohler, B. *Proc. Natl. Acad. Sci. U.S.A.* **2007**, *104*, 435.
(26) Sukowski, U.; Seilmeier, A.; Elsaesser, T.; Fischer, S. F. *J. Chem. Phys.* **1990**, *93*, 4094.
(27) Iwata, K.; Hamaguchi, H. *J. Phys. Chem. A* **1997**, *101*, 632.
(28) Hippler, H.; Troe, J.; Wendelken, H. J. *J. Chem. Phys.* **1983**, *78*, 5351.
(29) Schultz, K. E.; Russell, D. J.; Harris, C. B. *J. Chem. Phys.* **1992**, *97*, 5431.
(30) Bingemann, D.; King, A. M.; Crim, F. F. *J. Chem. Phys.* **2000**, *113*, 5018.
(31) Charvat, A.; Abmann, J.; Abel, B.; Schwarzer, D. *J. Phys. Chem. A* **2001**, *105*, 5071.
(32) Sension, R. J.; Repinec, S. T.; Hochstrasser, R. M. *J. Chem. Phys.* **1990**, *93*, 9185.
(33) Okazaki, T.; Hirota, N.; Terazima, M. *J. Chem. Phys.* **1999**, *110*, 11399.
(34) Schwarzer, D.; Kutne, P.; Schröder, C.; Troe, J. *J. Chem. Phys.* **2004**, *121*, 1754.
(35) Kwok, W.-M.; Ma, C.; Phillips, D. L. *J. Am. Chem. Soc.* **2006**, *128*, 11894.
(36) Tan, X.; Gustafson, T. L.; Lefumeux, C.; Burdzinski, G.; Buntinx, G.; Poizat, O. *J. Phys. Chem. A* **2002**, *106*, 3593.
(37) Matsika, S. *J. Phys. Chem. A* **2004**, *108*, 7584.
(38) Assmann, J.; Charvat, A.; Schwarzer, D.; Kappel, C.; Luther, K.; Abel, B. *J. Phys. Chem. A* **2002**, *106*, 5197.
(39) Yoo, H. S.; DeWitt, M. J.; Pate, B. H. *J. Phys. Chem. A* **2004**, *108*, 1365.
(40) Assmann, J.; von Benten, R.; Charvat, A.; Abel, B. *J. Phys. Chem. A* **2003**, *107*, 1904.
(41) Assmann, J.; von Benten, R.; Charvat, A.; Abel, B. *J. Phys. Chem. A* **2003**, *107*, 5291.
(42) Benniston, A. C.; Matousek, P.; McCulloch, I. E.; Parker, A. W.; Towrie, M. *J. Phys. Chem. A* **2003**, *107*, 4347.
(43) Cowan, M. L.; Bruner, B. D.; Huse, N.; Dwyer, J. R.; Chugh, B.; Nibbering, E. T. J.; Elsaesser, T.; Miller, R. J. D. *Nature* **2005**, *434*, 199.
(44) Ashihara, S.; Huse, N.; Espagne, A.; Nibbering, E. T. J.; Elsaesser, T. *J. Phys. Chem. A* **2007**, *111*, 743.
(45) Stenger, J.; Madsen, D.; Hamm, P.; Nibbering, E. T. J.; Elsaesser, T. *Phys. Rev. Lett.* **2001**, *87*, 027401.
(46) Xue, Y.; Xie, D.; Yan, G. *Int. J. Quantum Chem.* **2000**, *76*, 686.
(47) Fodor, S. P. A.; Rava, R. P.; Hays, T. R.; Spiro, T. G. *J. Am. Chem. Soc.* **1985**, *107*, 1520.
(48) Nitzan, A.; Jortner, J. *Mol. Phys.* **1973**, *25*, 713.
(49) Dlott, D. D. *Chem. Phys.* **2001**, *266*, 149.
(50) Deng, Y.; Stratt, R. M. *J. Chem. Phys.* **2002**, *117*, 1735.
(51) Morita, A.; Kato, S. *J. Chem. Phys.* **1998**, *109*, 5511.
(52) Shiga, M.; Okazaki, S. *J. Chem. Phys.* **1999**, *111*, 5390.
(53) Lim, M.; Gnanakaran, S.; Hochstrasser, R. M. *J. Chem. Phys.* **1997**, *106*, 3485.
(54) Chorny, I.; Vieceli, J.; Benjamin, I. *J. Chem. Phys.* **2002**, *116*, 8904.
(55) Hamm, P.; Lim, M.; Hochstrasser, R. M. *J. Chem. Phys.* **1997**, *107*, 10523.
(56) Alfano, J. C.; Kimura, Y.; Walhout, P. K.; Barbara, P. F. *Chem. Phys.* **1993**, *175*, 147.
(57) Paige, M. E.; Harris, C. B. *J. Chem. Phys.* **1990**, *93*, 1481.

(58) Buchvarov, I.; Wang, Q.; Raytchev, M.; Trifonov, A.; Fiebig, T. *Proc. Natl. Acad. Sci. U.S.A.* **2007**, *104*, 4794.
(59) Woutersen, S.; Cristalli, G. *J. Chem. Phys.* **2004**, *121*, 5381.
(60) Comeau, D.; Hache, A.; Melikechi, N. *Appl. Phys. Lett.* **2003**, *83*, 246.
(61) Matsunaga, N.; Nagashima, A. *J. Phys. Chem. Ref. Data* **1983**, *12*, 933.
(62) Lemmon, E. W.; McLinden, M. O.; Friend, D. G. Thermophysical Properties of Fluid Systems. In *NIST Chemistry WebBook*; NIST Standard Reference Database No. 69; Linstrom, P. J., Mallard, W. G. National Institute of Standards and Technology: Gaithersburg MD, June 2005 (http://webbook.nist.gov).
(63) Lide, D. R., Ed. *CRC Handbook of Chemistry and Physics*, Internet Version 2007 87th ed.; Taylor and Francis: Boca Raton, FL, 2007 (http://www.hbcpnetbase.com).